materials

MDPI

Article

Synthesis and Characterization of Lithium-Ion Conductive LATP-$LaPO_4$ Composites Using La_2O_3 Nano-Powder

Fangzhou Song [1], Masayoshi Uematsu [1], Takeshi Yabutsuka [1], Takeshi Yao [2] and Shigeomi Takai [1,*]

[1] Graduate School of Energy Science, Kyoto University, Yoshida-Honmachi, Sakyo-Ku, Kyoto 606-8501, Japan; song.fangzhou.48a@st.kyoto-u.ac.jp (F.S.); kagawa18@gmail.com (M.U.); yabutsuka@energy.kyoto-u.ac.jp (T.Y.)

[2] Kyoto University, Yoshida-Honmachi, Sakyo-Ku, Kyoto 606-8501, Japan; t_yao@hera.eonet.ne.jp

* Correspondence: stakai@energy.kyoto-u.ac.jp

Abstract: LATP-based composite electrolytes were prepared by sintering the mixtures of LATP precursor and La_2O_3 nano-powder. Powder X-ray diffraction and scanning electron microscopy suggest that La_2O_3 can react with LATP during sintering to form fine $LaPO_4$ particles that are dispersed in the LATP matrix. The room temperature conductivity initially increases with La_2O_3 nano-powder addition showing the maximum of 0.69 mS·cm^{-1} at 6 wt.%, above which, conductivity decreases with the introduction of La_2O_3. The activation energy of conductivity is not largely varied with the La_2O_3 content, suggesting that the conduction mechanism is essentially preserved despite $LaPO_4$ dispersion. In comparison with the previously reported LATP-LLTO system, although some unidentified impurity slightly reduces the conductivity maximum, the fine dispersion of $LaPO_4$ particles can be achieved in the LATP–La_2O_3 system.

Keywords: insulative particle dispersion; lithium-ion conductor; LATP; all-solid-state battery

Citation: Song, F.; Uematsu, M.; Yabutsuka, T.; Yao, T.; Takai, S. Synthesis and Characterization of Lithium-Ion Conductive LATP-$LaPO_4$ Composites Using La_2O_3 Nano-Powder. *Materials* **2021**, *14*, 3502. https://doi.org/10.3390/ma14133502

Academic Editor: Li Lu

Received: 31 May 2021
Accepted: 21 June 2021
Published: 23 June 2021

1. Introduction

The popularization of electric vehicles and mobile devices is calling for an advance in battery technology to meet the requirement on the battery reliability and higher energy density. Solid-state electrolytes (SSEs), with wider electrochemical window, nonflammability and low-temperature stability in comparison with the liquid counterparts, is a key component for the all-solid-state battery (ASSB) that is safer to use and allows more compact designs [1–4]. In recent decades, research has focused on the improvement of room temperature conductivities for SSEs, mainly through the development of new lithium-ion conductors or the improvement of currently available SSEs by means of doping or lattice tuning [1,3,5–9].

In addition to the above strategies, insulator particle dispersion has been explored to improve lithium-ion conduction, which was originally reported in C. Liang's work where Al_2O_3 particles were dispersed in LiI and resulted in 50 times enhancement in conductivity [10]. Similar phenomena were observed in subsequent research on halide-type lithium-ion conductors [11–16]. To explain the mechanism, various types of theories have been developed [17], among which, a space charge layer model originated by C. Wagner [18] is mostly accepted. According to this model, the charge carriers at the interface between ion conductor and insulative particles are redistributed due to the difference in chemical potentials, leading to deviation from electroneutrality to form the favorable region for the charge carrier to migrate [6,19–25]. Recent studies by means of NMR characterization also support the space charge layer model [26,27]. This strategy has been applied to a limited range of lithium-ion conductors such as halides and $LiBH_4$ [10–15,20–25,27–34]. Although it was recently reported that conductivity for oxide-based lithium-ion conductors can be increased by adding a secondary phase to modify the grain boundary conductivity [35–37],

relatively few studies have focused on the insulator particle dispersion strategy in oxide-based materials [38–41].

$Li_{1.3}Al_{0.3}Ti_{1.7}(PO_4)_3$ (LATP) is an oxide-based solid-state electrolyte with a rhombohedral NASICON-type structure that is composed of corner-sharing MO_6 (M = Ti or Al) octahedra and PO_4 tetrahedra, forming a three-dimensional diffusion network for lithium-ions within the lattice [1,3]. We have previously achieved 3 times improvement in room temperature conductivity by introducing $Li_{0.348}La_{0.55}TiO_3$ (LLTO) particles into the LATP matrix. The introduced LLTO reacted with the LATP matrix during the sintering process, forming fine $LaPO_4$ which act as insulative particles [40]. However, the direct introduction of $LaPO_4$ into LATP did not enhance the conductivity due to the growth of $LaPO_4$ particles [42]. In order to disperse the $LaPO_4$ particles finely through a simplified reaction, La_2O_3 nano-powder is selected as a more direct lanthanum source rather than LLTO particles. In this work, LATP–$LaPO_4$ composites are prepared by employing La_2O_3 nano-powder to compare with the results of the previous LLTO added system.

2. Materials and Methods

2.1. Synthesis of the LATP Precursor

$Li_{1.3}Al_{0.3}Ti_{1.7}(PO_4)_3$ (LATP) precursor was prepared by the solid-state reaction method. Stoichiometric amounts of Li_2CO_3 (99.0% Wako Pure Chem., Osaka, Japan, with 10 wt.% excess), γ-Al_2O_3 (97.0% Stream Chemical, Newburyport, MA, USA), TiO_2 (rutile, 99.9% High Purity Chem., Saitama, Japan) and $NH_4H_2PO_4$ (99.0% Wako Pure Chem., Osaka, Japan) were mixed in an automatic grinder for 5 h with an aid of ethanol. After drying for 24 h, the mixture was uniaxially pressed to form the green compact which was then calcined at 700 °C for 2 h. To form fine LATP precursor, the calcined product was crushed and ball-milled in zirconia pot with ethanol and zirconia balls for 5 h at 400 RPM (Pulverisette7 Premium Line, Fritsch, Idar-Oberstein, Germany).

2.2. Synthesis of the LATP–La_2O_3 Composite

To fabricate LATP-La_2O_3 composite pellets, the fine LATP precursor was mixed with La_2O_3 nano-powder (<100 nm, 99% Sigma-Aldrich, Hesse, Germany) by ball milling (zirconia balls and pot, Pulverisette7 Premium Line, Fritsch) with the aid of a small amount of ethanol for 1.5 h at 400 RPM. After drying, the powder mixture was isostatically pressed to form cylindrical pellets at 200 MPa followed by sintering at 1000 °C for 4 h. The sintering time was optimized according to the preliminarily examined sintering time dependence, as represented in Figures S1–S3 in the Supplementary Materials. In this work, the introduced La_2O_3 nano-powders were weighted 2, 4, 6, 8, 12 and 16 wt.% of the total weight (LATP + La_2O_3 mixture). Herein, the samples are referred as LATP–*x* wt.% La_2O_3, based on the amount of added La_2O_3.

2.3. Characterizations and Electrochemical Properties

The obtained crystalline phases were investigated by powder XRD on the Ultima VI diffractometer (Rigaku, Tokyo, Japan) using a CuKα radiation source (40 kV, 40 mA). The microstructure and particle distribution of the samples were observed by scanning electron microscopy under the back-scattering electron mode (SEM, SU6600, Hitachi, Tokyo, Japan). The sample pellets with a 6 mm diameter and 3 mm thickness were polished on both sides and sputtered with gold to form electrodes. To investigate the temperature variation of electrochemical impedance, the samples were clamped in a 4-electrode test apparatus in a temperature-controlled tubular furnace. An amount of 0.5 V of AC potential was applied to the sample pellets using an LRC meter (3531 Z Hitester, Hioki, Japan) in a frequency range of 130 Hz–1.3 MHz and a temperature range of 25–200 °C. The conductivities were calculated by the equivalent circuit fitting from the impedance spectroscopies using ZView® software (Scribner, New York, NA, USA) [43].

3. Results and Discussions

Powder XRD pattern of LATP ($Li_{1.3}Al_{0.3}Ti_{1.7}(PO_4)_3$) and LATP–$x$ wt.% La_2O_3 composites are shown in Figure 1, where the major peaks are associated with LATP that is isostructural with $LiTi_2(PO_4)_3$. The existence of $LaPO_4$ (labelled by solid inverted triangle) suggests a solid-state reaction between the LATP matrix and introduced La_2O_3 during sintering. $LaPO_4$ formation at the sintering also occurred in LATP-LLTO and LAGP-LLTO systems in the previous works [40,41]. In addition to $LaPO_4$ formation, a $LiTiPO_5$ phase and an unidentified impurity were also observed in the powder XRD patterns, as labelled by hollow diamonds and hollow inverted triangles in Figure 1. The small amount of $LiTiPO_5$ phase is believed to be formed during sintering when the LATP matrix donates phosphorus to form $LaPO_4$. The $LiTiPO_5$ and unidentified impurities constantly remained despite prolonged sintering, as observed in Figure S1, for the LATP–8 wt.% La_2O_3 system.

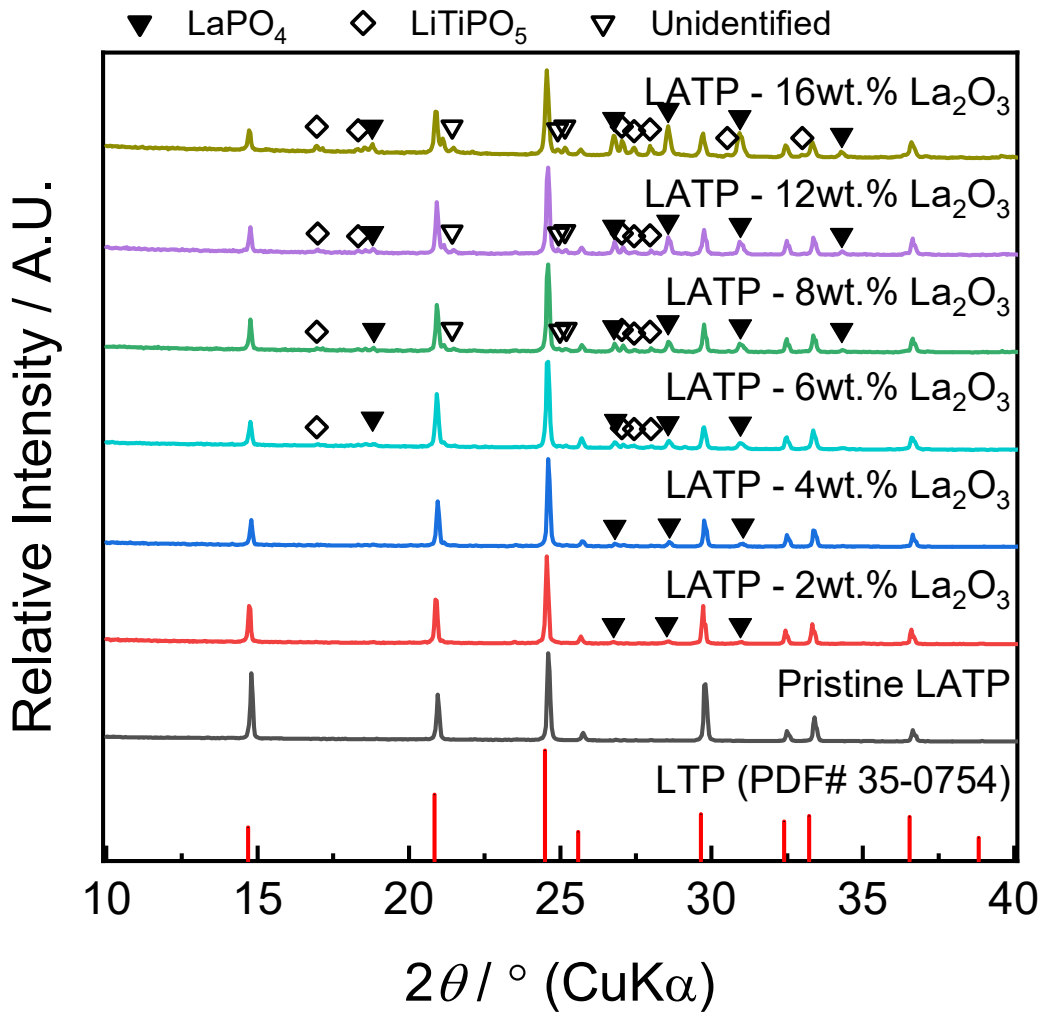

Figure 1. Powder XRD patterns of pristine LATP and LATP–La_2O_3 composites. $LaPO_4$, $LiTiPO_5$ and unidentified phases are labelled by solid inverted triangle, hollow diamond, and hollow inverted triangle, respectively.

Figure 2 presents SEM images of pristine LATP and composite samples captured under back-scattered electron mode, where the bright spots represent the lanthanum-containing particles due to the heaver atom. For relatively smaller La_2O_3 addition below 8 wt.%, the dispersed particles are isolated, keeping the similar sizes, as shown in Figure 2b–d. At higher La_2O_3 additions such as 12 or 16 wt.%, the particles are aggregated to break the percolation of LATP matrix, as shown in Figure 2e,f.

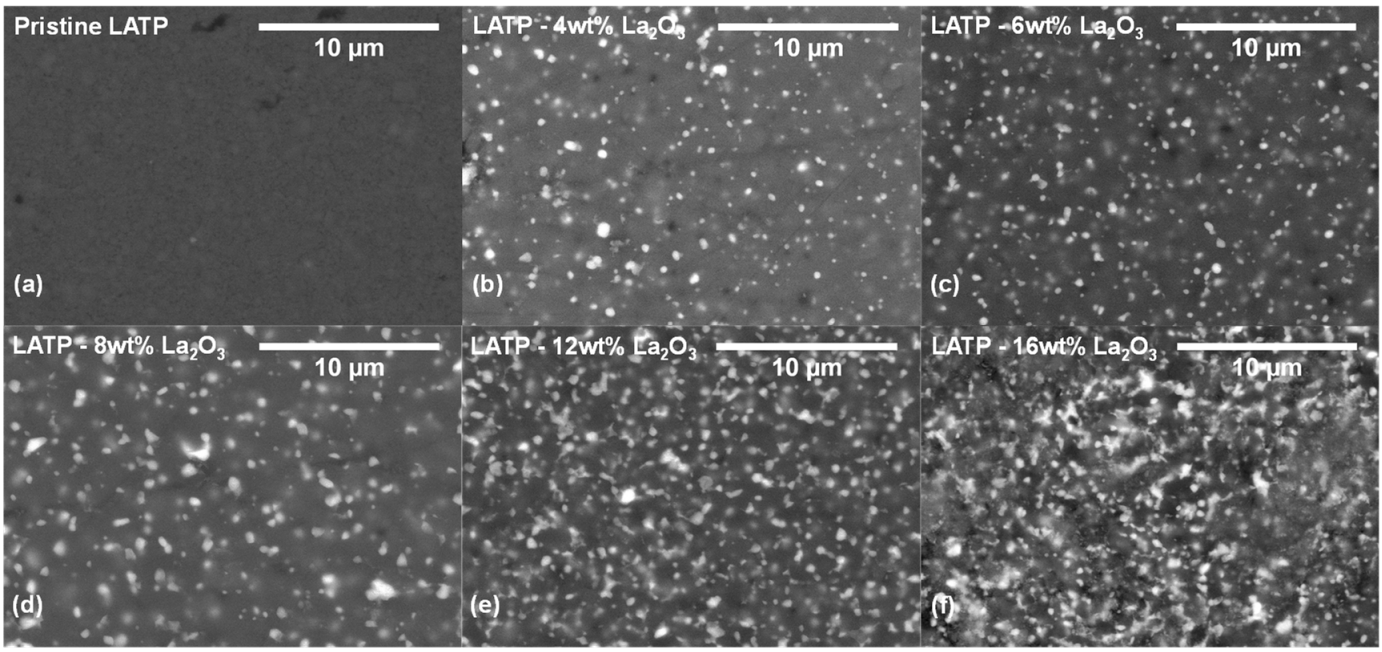

Figure 2. Back-scattering SEM images of (**a**) pristine LATP, (**b**) LATP–4 wt.%, (**c**) LATP–6 wt.%, (**d**) LATP–8 wt.%, (**e**) LATP–12 wt.%, and (**f**) LATP–16 wt.% La_2O_3.

The Nyquist plots of electrochemical impedance spectroscopies for pristine LATP and composite samples are shown in Figure 3. Owing to the limited frequency range, the impedance spectra are fitted by using a conventional equivalent circuit in the inset to obtain the right side of the semi-circles as the total resistivity. The room temperature conductivities of the samples are presented as a function of La_2O_3 addition in Figure 4, where the highest conductivity of 0.69 mS·cm^{-1} is achieved at 6 wt.% of La_2O_3 addition. This suggests that the addition of La_2O_3 nano-powder can form $LaPO_4$ particles in LATP matrix. From 6 wt.% up to 16 wt.% of La_2O_3 introduction, the conductivity decreases with the La_2O_3 addition. This is caused by the aggregation of the insulative particles, which severely block the migration of the lithium-ions in the LATP matrix to reduce the total conductivity.

For comparison, the conductivity of previous LATP–LLTO composites [40] are also plotted in Figure 4 (hollow triangles). The weight percentage of LLTO is converted to the equivalent amount of La_2O_3 based on the lanthanum content in additives. Although the highest conductivity in this work is slightly smaller than the previously observed 0.76 mS·cm^{-1} in LATP–4 wt.% LLTO [40], about three-fold enhancement from the pristine can be achieved. The slightly smaller conductivity might be due to the unidentified impurity, which could block the LATP matrix/$LaPO_4$ particle interface. It should be noted that the maximum conductivity occurs at higher lanthanum content in comparison with the previous LATP–LLTO system, indicating that La_2O_3 nano-powder is effective in forming finely dispersed $LaPO_4$ particles without aggregation. Suppressing the formation of unidentified impurity should be critical for further enhancement in conductivity.

The conductivities are plotted against inverse temperature, as shown in Figure 5a, which can be linearly fitted to the Arrhenius equation $\sigma_T T = \sigma_0 \exp(-E_a/kT)$, where σ_T, σ_0 and E_a denote the total conductivity, pre-exponential term and the activation energy, respectively. The deduced activation energy is plotted as a function of La_2O_3 addition in Figure 5b. The activation energies are similar to pristine LATP or slightly increased with the introduction of La_2O_3 nano-powder, suggesting that the lithium migration mechanism of composite is essentially consistent with that of pristine LATP.

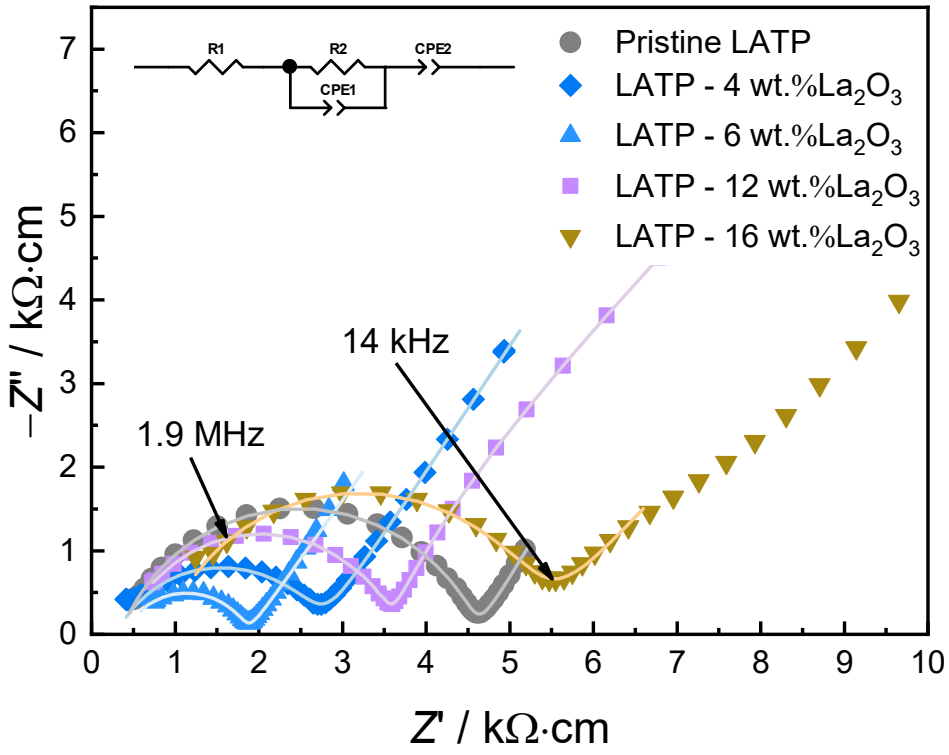

Figure 3. Nyquist plots of pristine LATP and composite samples with fitted curves. The related equivalent circuit is shown in the inset.

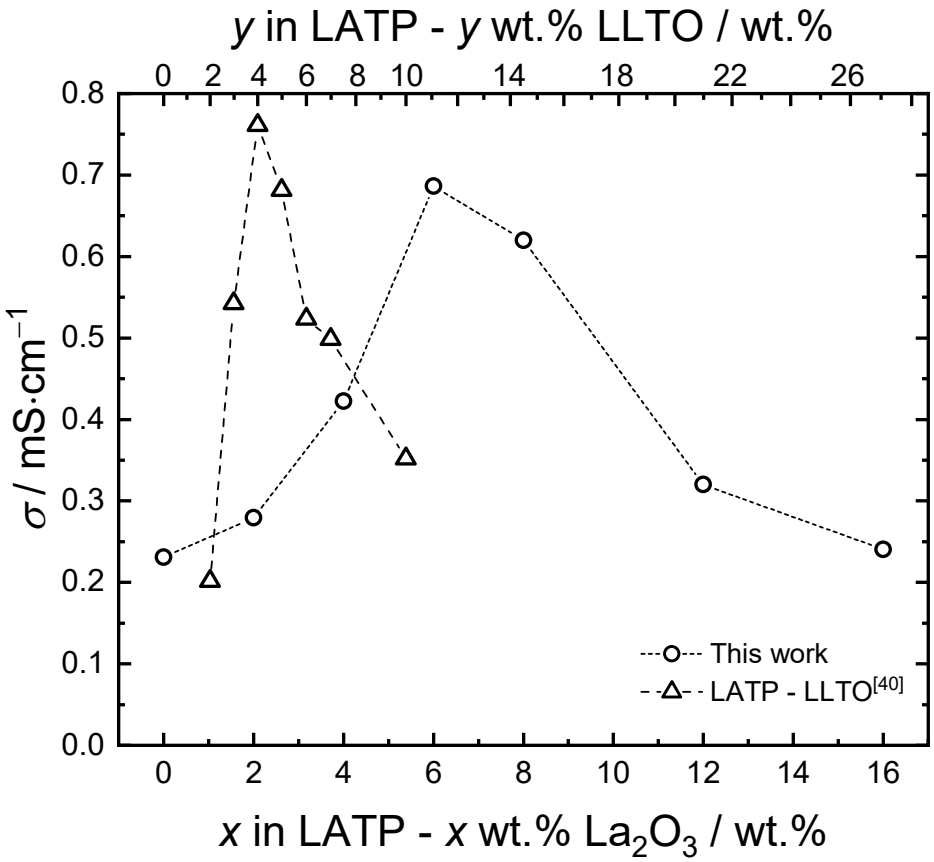

Figure 4. Room temperature conductivity of LATP–x wt.% La_2O_3 as a function of La_2O_3 addition, in comparison with the results in LATP–y wt.% LLTO from the previous work [40].

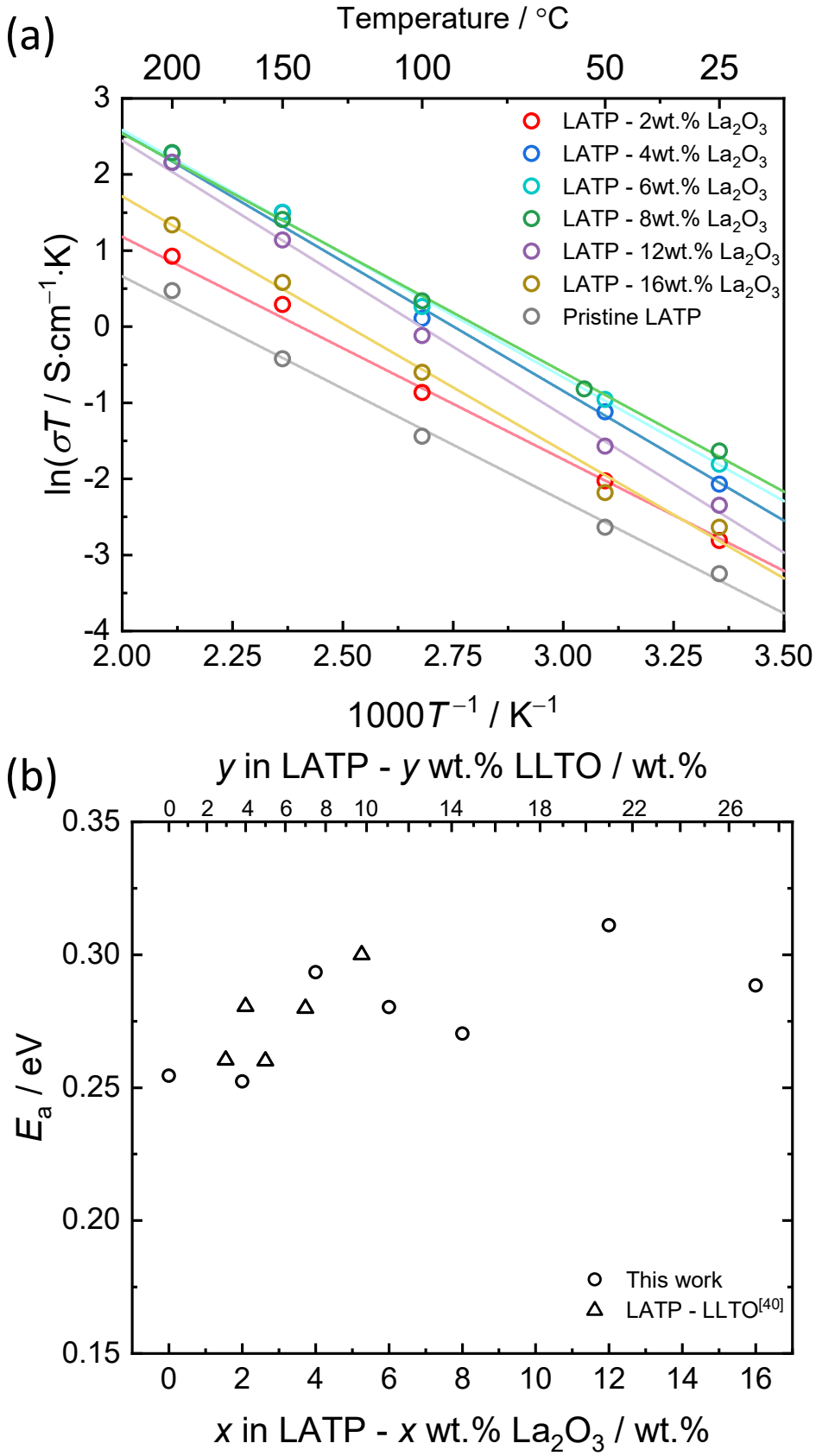

Figure 5. (**a**) Arrhenius plots of LATP–x wt.% La_2O_3, and (**b**) activation energies of LATP–x wt.% La_2O_3 compared with the results of the previous work [40].

In summary, by adding La_2O_3 nano-powder into the LATP precursor, $LaPO_4$ particles can be dispersed into the LATP matrix through solid-state reaction during sintering process. A three-fold enhancement in conductivity is observed in the LATP–6 wt.% La_2O_3 sample, while the activation energy of the composite is not largely different from the pristine LATP. In further study, characterizations such as ^{7}Li solid-state NMR spectroscopy and high-resolution transmission electron microscopy are required to scrutinize the lithium-ion conduction mechanism and microstructural features at the LATP matrix/$LaPO_4$ particle interface.

4. Conclusions

In this work, LATP-based composite electrolytes were synthesized by adding La_2O_3 nano-powder into an LATP precursor. Powder XRD and back-scattered SEM prove that $LaPO_4$ particles were formed to disperse in the sintered samples during sintering. The aggregation of particles is observed at higher lanthanum introduction. The room temperature conductivity of the composite electrolytes increases with the La_2O_3 addition until 6 wt.%, where the maximum conductivity of 0.69 mS·cm^{-1} is achieved, which is ascribed to the insulative particle dispersion effect. In comparison with the previous study on the LATP–LLTO composites [40], the maximum conductivity is observed at the higher lanthanum content, although the maximum conductivity is inferior to the previous one. Further improvement is expected through the elimination of impurities. The compositional dependence of activation energies of conductivity suggests that the present LATP-La_2O_3 system possesses a similar conduction mechanism to the previous LATP-LLTO system.

Supplementary Materials: The following are available online at https://www.mdpi.com/article/10.3390/ma14133502/s1, Figure S1: powder XRD pattern of LATP–8 wt.% La_2O_3 sample with sintering times ranging from 1 to 10 h, the unidentified impurity peaks are labelled by hollow inverted triangles. Figure S2: back-scattered SEM images of LATP–8 wt.% La_2O_3 samples with different sintering times. Figure S3: conductivity of LATP–8 wt.% La_2O_3 as a function of sintering time.

Author Contributions: Conceptualization, S.T.; validation, F.S. and M.U.; formal analysis, F.S. and M.U.; investigation, F.S. and M.U.; resources, S.T.; data curation, F.S. and M.U.; writing—original draft preparation, F.S.; writing—review and editing, F.S. and S.T.; visualization, F.S. and M.U.; supervision, T.Y. (Takeshi Yabutsuka) and T.Y. (Takeshi Yao); project administration, S.T.; funding acquisition, S.T. All authors have read and agreed to the published version of the manuscript.

Funding: This work was partly supported by ISHIZUE 2020 of Kyoto University Research Development Program.

Institutional Review Board Statement: Not applicable.

Informed Consent Statement: Not applicable.

Data Availability Statement: The data presented in this study are available on request from the corresponding author.

Conflicts of Interest: The authors declare no conflict of interest.

References

1. Gao, Z.; Sun, H.; Fu, L.; Ye, F.; Zhang, Y.; Luo, W.; Huang, Y. Promises, challenges, and recent progress of inorganic solid-state electrolytes for all-solid-state lithium batteries. *Adv. Mater.* **2018**, *30*, 1705702. [CrossRef] [PubMed]
2. Zhang, Z.; Shao, Y.; Lotsch, B.; Hu, Y.-S.; Li, H.; Janek, J.; Nazar, L.F.; Nan, C.-W.; Maier, J.; Armand, M.; et al. New horizons for inorganic solid state ion conductors. *Energy Environ. Sci.* **2018**, *11*, 1945–1976. [CrossRef]
3. Zheng, F.; Kotobuki, M.; Song, S.; Lai, M.O.; Lu, L. Review on solid electrolytes for all-solid-state lithium-ion batteries. *J. Power Sources* **2018**, *389*, 198–213. [CrossRef]
4. Famprikis, T.; Canepa, P.; Dawson, J.A.; Islam, M.S.; Masquelier, C. Fundamentals of inorganic solid-state electrolytes for batteries. *Nat. Mater.* **2019**, 1–14. [CrossRef] [PubMed]
5. Goodenough, J.B.; Kim, Y. Challenges for rechargeable Li batteries. *Chem. Mater.* **2010**, *22*, 587–603. [CrossRef]
6. Maier, J. Pushing nanoionics to the limits: Charge carrier chemistry in extremely small systems. *Chem. Mater.* **2014**, *26*, 348–360. [CrossRef]

7. Hao, S.; Zhang, H.; Yao, W.; Lin, J. Solid-state lithium battery chemistries achieving high cycle performance at room temperature by a new garnet-based composite electrolyte. *J. Power Sources* **2018**, *393*, 128–134. [CrossRef]
8. Thangadurai, V.; Narayanan, S.; Pinzaru, D. Garnet-type solid-state fast Li ion conductors for Li batteries: Critical review. *Chem. Soc. Rev.* **2014**, *43*, 4714–4727. [CrossRef]
9. Xiao, R.; Li, H.; Chen, L. Candidate structures for inorganic lithium solid-state electrolytes identified by high-throughput bond-valence calculations. *J. Mater.* **2015**, *1*, 325–332. [CrossRef]
10. Liang, C.C. Conduction Characteristics of the Lithium Iodide-Aluminum Oxide Solid Electrolytes. *J. Electrochem. Soc.* **1973**, *120*, 1289. [CrossRef]
11. Uvarov, N.F.; Isupov, V.P.; Sharma, V.; Shukla, A.K. Effect of morphology and particle size on the ionic conductivities of composite solid electrolytes. *Solid State Ionics* **1992**, *51*, 41–52. [CrossRef]
12. Maier, J. Heterogeneous doping of silver bromide (AgBr: Al_2O_3). *Mater. Res. Bull.* **1985**, *20*, 383–392. [CrossRef]
13. Maier, J. On the heterogeneous doping of ionic conductors. *Solid State Ionics* **1986**, *18*, 1141–1145. [CrossRef]
14. Schoonman, J.; Poulsen, F.W.; Andersen, N.H.; Kindl, B. Properties of LiI-Alumina composite electrolytes. *Solid State Ionics* **1983**, *9*, 119–122. [CrossRef]
15. Khandkar, A.C.; Wagner, J.B., Jr. Fast ion transport in composites. *Solid State Ionics* **1986**, *18*, 1100–1104. [CrossRef]
16. Shahi, K.; Wagner, J.B., Jr. Enhanced ionic conduction in dispersed solid electrolyte systems (DSES) and/or multiphase systems: AgI-Al_2O_3, AgI-SiO_2, AgI-Fly ash, and AgI-AgBr. *J. Solid State Chem.* **1982**, *42*, 107–119. [CrossRef]
17. Agrawal, R.C.; Gupta, R.K. Superionic solid: Composite electrolyte phase–an overview. *J. Mater. Sci.* **1999**, *34*, 1131–1162. [CrossRef]
18. Wagner, C. The electrical conductivity of semi-conductors involving inclusions of another phase. *J. Phys. Chem. Solids* **1972**, *33*, 1051–1059. [CrossRef]
19. Heitjans, P.; Wilkening, M. Ion dynamics at interfaces: Nuclear magnetic resonance studies. *MRS Bull.* **2009**, *34*, 915–922. [CrossRef]
20. Sultana, S.; Rafiuddin, R. Enhancement of ionic conductivity in the composite solid electrolyte system: TlI–Al_2O_3. *Ionics* **2009**, *15*, 621–625. [CrossRef]
21. Knauth, P. Inorganic solid Li ion conductors: An overview. *Solid State Ionics* **2009**, *180*, 911–916. [CrossRef]
22. Gulino, V.; Barberis, L.; Ngene, P.; Baricco, M.; de Jongh, P.E. Enhancing Li-Ion Conductivity in $LiBH_4$-Based Solid Electrolytes by Adding Various Nanosized Oxides. *ACS Appl. Energy Mater.* **2020**, *3*, 4941–4948. [CrossRef]
23. Zou, Z.; Li, Y.; Lu, Z.; Wang, D.; Cui, Y.; Guo, B.; Li, Y.; Liang, X.; Feng, J.; Li, H.; et al. Mobile Ions in Composite Solids. *Chem. Rev.* **2020**, *120*, 4169–4221. [CrossRef] [PubMed]
24. Epp, V.; Wilkening, M. Motion of Li^+ in nanoengineered $LiBH_4$ and $LiBH_4$: Al_2O_3 comparison with the microcrystalline form. *ChemPhysChem* **2013**, *14*, 3706–3713. [CrossRef] [PubMed]
25. Maier, J. Ionic conduction in space charge regions. *Prog. Solid State Chem.* **1995**, *23*, 171–263. [CrossRef]
26. Breuer, S.; Pregartner, V.; Lunghammer, S.; Wilkening, H.M.R. Dispersed solid conductors: Fast interfacial Li-ion dynamics in nanostructured LiF and LiF: γ-Al_2O_3 composites. *J. Phys. Chem. C* **2019**, *123*, 5222–5230. [CrossRef]
27. Lefevr, J.; Cervini, L.; Griffin, J.M.; Blanchard, D. Lithium Conductivity and Ions Dynamics in $LiBH_4/SiO_2$ Solid Electrolytes Studied by Solid-State NMR and Quasi-Elastic Neutron Scattering and Applied in Lithium–Sulfur Batteries. *J. Phys. Chem. C* **2018**, *122*, 15264–15275. [CrossRef]
28. Indris, S.; Heitjans, P.; Roman, H.E.; Bunde, A. Nanocrystalline versus microcrystalline Li_2O: B_2O_3 composites: Anomalous ionic conductivities and percolation theory. *Phys. Rev. Lett.* **2000**, *84*, 2889. [CrossRef]
29. Albinet, G.; Debierre, J.M.; Knauth, P.; Lambert, C.; Raymond, L. Enhanced conductivity in ionic conductor-insulator composites: Numerical models in two and three dimensions. *Eur. Phys. J. B-Condens. Matter Complex Syst.* **2001**, *22*, 421–427. [CrossRef]
30. Wilkening, M.; Indris, S.; Heitjans, P. Heterogeneous lithium diffusion in nanocrystalline Li_2O: Al_2O_3 composites. *Phys. Chem. Chem. Phys.* **2003**, *5*, 2225–2231. [CrossRef]
31. Bhattacharyya, A.J.; Dollé, M.; Maier, J. Improved Li-battery electrolytes by heterogeneous doping of nonaqueous Li-salt solutions. *Electrochem. Solid State Lett.* **2004**, *7*, A432. [CrossRef]
32. Ulrich, M.; Bunde, A.; Indris, S.; Heitjans, P. Li ion transport and interface percolation in nano-and microcrystalline composites. *Phys. Chem. Chem. Phys.* **2004**, *6*, 3680–3683. [CrossRef]
33. Indris, S.; Heitjans, P.; Ulrich, M.; Bunde, A. AC and DC conductivity in nano-and microcrystalline Li_2O: B_2O_3 composites: Experimental results and theoretical models. *Z. Phys. Chem.* **2005**, *219*, 89–103. [CrossRef]
34. Gulino, V.; Brighi, M.; Murgia, F.; Ngene, P.; de Jongh, P.; Černý, R.; Baricco, M. Room-Temperature Solid-State Lithium-Ion Battery Using a $LiBH_4$–MgO Composite Electrolyte. *ACS Appl. Energy Mater.* **2021**, *4*, 1228–1236. [CrossRef]
35. Kwatek, K.; Ślubowska, W.; Ruiz, C.; Sobrados, I.; Sanz, J.; Garbarczyk, J.E.; Nowiński, J.L. The mechanism of enhanced ionic conductivity in $Li_{1.3}Al_{0.3}Ti_{1.7}(PO_4)_3$–($0.75Li_2O{\cdot}0.25B_2O_3$) composites. *J. Alloys Compd.* **2020**, *838*, 155623. [CrossRef]
36. Kwatek, K.; Ślubowska, W.; Trébosc, J.; Lafon, O.; Nowiński, J.L. Structural and electrical properties of ceramic Li-ion conductors based on $Li_{1.3}Al_{0.3}Ti_{1.7}(PO_4)_3$-LiF. *J. Eur. Ceram. Soc.* **2020**, *40*, 85–93. [CrossRef]
37. Hupfer, T.; Bucharsky, E.C.; Schell, K.G.; Hoffmann, M.J. Influence of the secondary phase $LiTiOPO_4$ on the properties of $Li_{1+x}Al_xTi_{2-x}(PO_4)_3$ (x= 0; 0.3). *Solid State Ionics* **2017**, *302*, 49–53. [CrossRef]

38. Saito, Y.; Mayne, J.; Ado, K.; Yamamoto, Y.; Nakamura, O. Electrical conductivity enhancement of $Na_4Zr_2Si_3O_{12}$ dispersed with ferroelectric $BaTiO_3$. *Solid State Ionics* **1990**, *40*, 72–75. [CrossRef]
39. Mei, A.; Wang, X.-L.; Feng, Y.-C.; Zhao, S.-J.; Li, G.-J.; Geng, H.-X.; Lin, Y.-H.; Nan, C.-W. Enhanced ionic transport in lithium lanthanum titanium oxide solid state electrolyte by introducing silica. *Solid State Ionics* **2008**, *179*, 2255–2259. [CrossRef]
40. Onishi, H.; Takai, S.; Yabutsuka, T.; Yao, T. Synthesis and electrochemical properties of LATP-LLTO lithium ion conductive composites. *Electrochemistry* **2016**, *84*, 967–970. [CrossRef]
41. Song, F.; Yamamoto, T.; Yabutsuka, T.; Yao, T.; Takai, S. Synthesis and Characterization of LAGP-Based Lithium Ion-Conductive Composites with an LLTO Additive. *J. Alloys Compd.* **2021**, *853*. [CrossRef]
42. Takai, S.; Yabutsuka, T.; Yao, T. Synthesis and ion conductivity enhancement in oxide-based solid electrolyte LLZ-LLTO and LATO-LLTO compsite (in Japanese). In *Development of Technology, Materials and Fabrication Process in Improving Ion Conductivity in All Solid State Batteries*; Technical Information Institute: Tokyo, Japan, 2017; pp. 74–80.
43. Johnson, D. *ZView: A Software Program for IES Analysis, Version 2.8*; Scribner Assoc. Inc.: South. Pines, NC, USA, 2002.